J Mater Sci (2011) 46:2578–2586
DOI 10.1007/s10853-010-5110-3

Surface modifications of talcs. Effects of inorganic and organic acid treatments

Luciana A. Castillo · Silvia E. Barbosa · Pedro Maiza · Numa J. Capiati

Received: 5 July 2010 / Accepted: 23 November 2010 / Published online: 7 December 2010

Abstract A multipurpose acid treatment, which comprises purification, delamination, particle size reduction, and surface modification on milled talc samples, is proposed. Talcs of different origins and composition were studied in order to assess and compare the effects of different acid treatments. Associated minerals were dissolved away by both inorganic and monocarboxylic organic acids, rendering more pure and lower particle size talcs. The main results obtained from hydrochloric acid treatment were purified talcs, having silanol groups onto their surfaces. This treatment allowed the complete removal of carbonates and chlorite from initial talcs, allowing for a length and thickness reduction of talc particles and the change to hydrophilic character by breakage of siloxane bonds. The so-treated talc achieved a purity level enough to be used in plastic and paper industry, paints among other upgraded talc applications. On the other hand, organic acid attacks were able to graft carboxylic groups onto the talc surface. The occurrence of this reaction was verified by independent characterization techniques both direct (Fourier Transform Infrared Spectroscopy, Energy Dispersive X-ray) and indirect (X-ray Diffraction, Scanning Electronic Microscopy, hydrophobicity/hydrophilicity test).

L. A. Castillo · S. E. Barbosa (✉) · N. J. Capiati
Planta Piloto de Ingeniería Química, UNS—CONICET,
Camino La Carrindanga Km. 7, Bahía Blanca, Argentina
e-mail: sbarbosa@plapiqui.edu.ar

P. Maiza
Departamento de Geología, UNS, Av. Alem 1253,
8000 Bahía Blanca, Argentina

Introduction

Addition of inorganic particulate fillers to commercial thermoplastic resins is a simple and commonly used alternative to tailor their properties and to reduce processing costs. Incorporation of fillers can affect the properties due to their chemical nature, particle size, shape and distribution, as well as its presence in the composite matrix that can be induced by their presence [1, 2].

Talc is a low cost layered silicate (phyllosilicate) and it has been used as filler to improve mechanical properties and macromolecular orientation of polypropylene (PP) [3–6].

PP/talc composites can become relatively low cost materials having improved flow, diffusive and mechanical properties respect to pure PP [7]. In particular, talc layers have a notable nucleating effect on PP crystallization, greater than other fillers of like composition and structure, i.e., pyrophyllite [8, 9]. Also, the nucleating ability of talc depends on its particle size and distribution in the matrix. Smaller and more delaminated (lower thickness) particles induce greater changes and better properties in the matrix [10, 11]. On the other side, the non-polar nature of PP is incompatible with the essentially polar character exhibited by mineral particles. This may cause poor particle dispersion and wetting, low interfacial particle–matrix strength, and decreased fracture resistance, especially in highly filled composites [12]. For this, final properties of PP/talc composites are improved by reducing talc particle size and by increasing matrix–filler contact area and compatibility. These conditions can be achieved by a proper delamination and superficial modification of talc particles.

In this study, a multipurpose acid treatment, which comprises purification, delamination, particle size reduction, and surface modification on milled talc samples, is

proposed. Associated minerals are dissolved away by both inorganic and monocarboxylic organic acids, rendering more pure and lower particle size talcs.

Experimental

Materials

Talc samples from two different origins were used: high purity Australian talc (A10) and Argentinean talc (SJ10), with up to 16% impurities. Acetic acid (CH_3COOH) 99.5% purity from Laboratorio Cicarelli, formic acid (HCOOH) 99% pro analysis from Anedra, and hydrochloric acid (HCl) 37% ISO pro analysis from Carlo Erba were used in this study.

Surface modification reactions

Acid treatment on talc was carried out in a 2 L glass reactor, heated to 80 ± 2 °C for 2 h. The treated talc was then filtered, washed with distilled water, and dried in a vacuum oven at 70 °C for 48 h. All the experiences were run at a concentration of 100 g of talc per L of acid solution. Table 1 resumes treatment conditions and reaction products name.

Characterization

Talc mineral samples were subjected to a detailed characterization before and after acid treatments. Polarized Light Optical Microscopy (OM) of thin cuts was employed to identify the presence of associated minerals and their distributions in the initial talcs. Chemical bonds were determined by Fourier Transform Infrared Spectroscopy (FTIR). A Nicolet 520 spectrophotometer was used. The spectra were obtained in the range from 400 to 4000 cm^{-1}, running 100 scans at a resolution of 4 cm^{-1}. The samples were diluted in potassium bromide (KBr) using two different concentrations (2 and 0.2 wt%) to analyze OH stretching and Si vibrations, respectively. X-ray Diffraction (XRD) was used to identify crystal structures. Diffraction patterns were obtained in a Rigaku DMAX III C diffractometer at 35 kV and 15 mA, with a Ni filter, CuK, and graphite monochromator. The 2θ values ranged from 3° to 60°. The structural alteration due to the acid treatment was determined by the crystallinity index (C), as defined by Ohlberg and Strickler [13]. The C index was calculated by $C = (B_0\, I/B\, I_0) \times 100\%$, where I_0 and B_0 are the peak and background intensity of initial talcs, and I and B are the peak and background intensities of treated talcs, respectively. Talc particle size was assessed by using a combination of electron microscopy techniques. The data processing was carried out with an Analysis PRO™ software package. About 100 particles were considered to calculate length, thickness, and their standard deviation (σ). Particle thickness was determined by Transmission Electron Microscopy (TEM). Micrographs were obtained in a JEOL 100 CX instrument at 100 kV. The talc samples were included in a resin and then sectioned in a Leica Ultracryomicrotome. The particle length as well as the morphology were determined by Scanning Electron Microscopy (SEM) in a JEOL 35 CF instrument, equipped with an Energy Dispersive X-ray (EDX) microanalyzer to sense the local distribution of elements. A qualitative test of hydrophobic/hydrophilic talc character was carried out by adding 1 g of talc into a pair of liquids of different polarity and density (hexane and water). Particle migration was observed after a settling time of 1 h.

Table 1 Molar concentration, pH and name of talcs for each acid treatment

Acid	Name	Molar concentration	pH
HCl	A10-C/SJ10-C	0.022	−1.1
HCOOH	A10-F/SJ10-F	0.010	1.17
CH_3COOH	A10-A/SJ10-A/SJ10-CA*	0.015	1.76

* SJ10-CA is the talc obtained from the reaction between SJ10-C and CH_3COOH

Results and discussion

Characterization of initial talcs

Figure 1 reveals thin cut sample micrographs of initial talcs, obtained by polarized light OM. In the A10 micrograph (Fig. 1a), massive talc was observed along with some chlorite spots of general formula $Mg_5(A1,Fe)(A1,Si)_4O_{10}(OH)_8$. Instead, the SJ10 sample (Fig. 1b) consisted in a random intergrowth of associated minerals, like veins of carbonates and chlorite among talc layers. Also, the grain size and associated minerals content of A10 were much lower than the corresponding SJ10.

The FTIR spectra from A10 and SJ10 are presented in Fig. 2. The bands corresponding to talc and associated minerals were indentified for clarity. A comparative analysis was done, especially in the regions where OH stretching (4000–2500 cm^{-1}) and Si vibration (1200–400 cm^{-1}) bands are located. In the A10 spectrum (Fig. 2a) dolomite ($CaMg(CO_3)_2$) and chlorite were present, while the SJ10 spectrum (Fig. 2b) revealed the presence of chlorite and various carbonates like dolomite, calcite ($CaCO_3$), and magnesite ($MgCO_3$).

The results of crystallographic characterization by XRD of A10 and SJ10 are presented in Fig. 3. The A10 sample

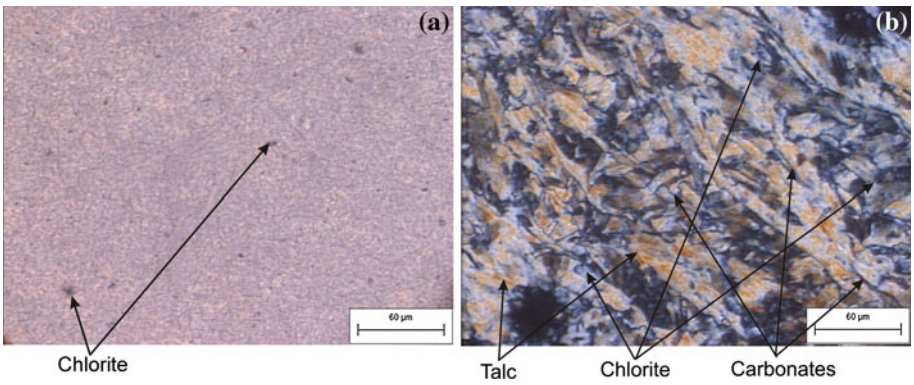

Fig. 1 Optical micrographs from thin cuts of initial talcs using cross polarized light: **a** A10 and **b** SJ10

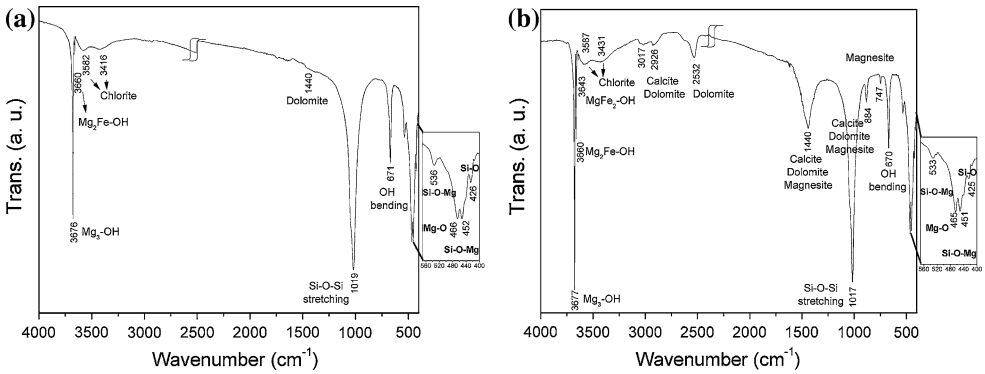

Fig. 2 FTIR spectra of initial talcs: **a** A10 and **b** SJ10

(Fig. 3a) contained the typical talc reflections corresponding to the basal planes (001), (002), and (003) in 9.32, 4.68 and 3.12 Å, respectively. Also, a neat dolomite reflection appeared. Figure 3b confirmed the greater content of associated minerals in SJ10 respect to A10, in agreement with FTIR analysis.

Morphological features of the two studied talcs are presented in Fig. 4, along with the corresponding EDX spectra. A10 showed two types of particles; the larger ones (Fig. 4a) were rounded in shape, organized in laminar concentric domains (onion-like), and anisotropic. These particles tend to disaggregate upon milling, giving smaller laminar particles. As expected, the EDX spectrum (Fig. 4c) showed the talc elements: Si (1.8 keV), Mg (1.2 keV), and O (0.5 keV), but also a small peak of C at 0.3 keV, which came from dolomite. On the other side, SJ10 particles appeared as blocks, with abrupt and well-defined borders. Layers, which were grouped within the blocks, got curved upon delamination and separated by one of their ends like the sheets of a book (Fig. 4b). The EDX spectrum in Fig. 4d revealed, besides Si, Mg, and O, the elements Ca (3.7 keV), Fe (6.4 keV), and C (0.3 keV) corresponding to the associated minerals. The C peak observed was much higher than the one showed by the A10 sample, as could be expected from the larger amount of impurities of SJ10, particularly carbonates.

Talc surface modification

Talc particles, as showed in Fig. 5, have two types of surfaces originated during milling: one that is a consequence of interlaminar slippage, named "face" and the other, generated by ionic bonds breakage, called "edge" [14]. The face surfaces are formed by almost compensated oxygen atoms, having low electrical charge and behaving as non-polar in water. These are low energy surfaces, containing basic and hydrophobic groups like siloxanes (–Si–O–Si–). On the other side, the edge surfaces include OH, Si, O, and Mg ions. They hold relatively high electrical charge, are polar in water, and present acid and hydrophilic groups as silanols (–SiOH) as well as basic groups as –MgOH [15].

The results of inorganic and organic acid treatments on final surface of both initial talcs were presented and discussed comparatively. Figure 6 included FTIR spectra from A10 and SJ10 treated with inorganic and organic acids. In A10-A, the bands at 2926 and 2854 cm^{-1} were assigned to asymmetric vibrations of C–H bonds (A10-A in Fig. 6a). These bonds are part of the functional groups attached to the talc surface on account of the reaction with acetic acid. Organic bands were also observed for talcs modified by formic acid (A10-F in Fig. 6a). When talc was treated with HCl the –OH group vibration, having strong

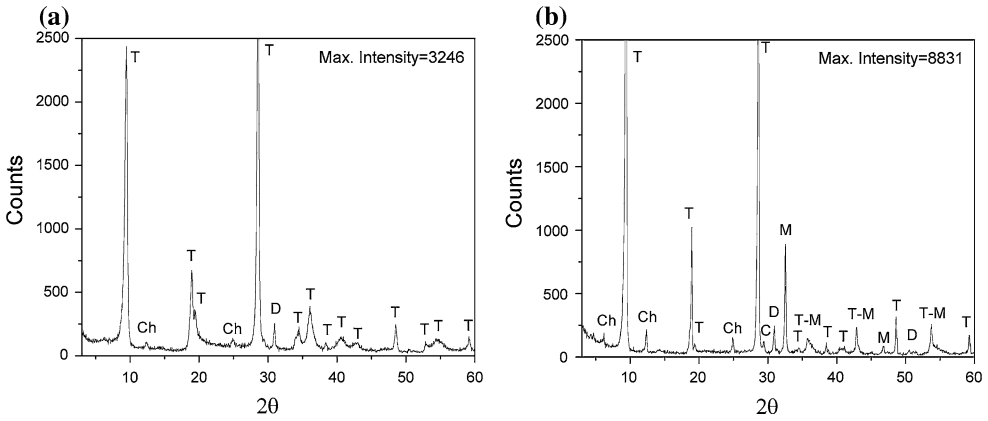

Fig. 3 XRD spectrum of initial talcs: **a** A10 and **b** SJ10. *T* talc, *D* dolomite, *C* calcite, *Ch* chlorite, *M* magnesite

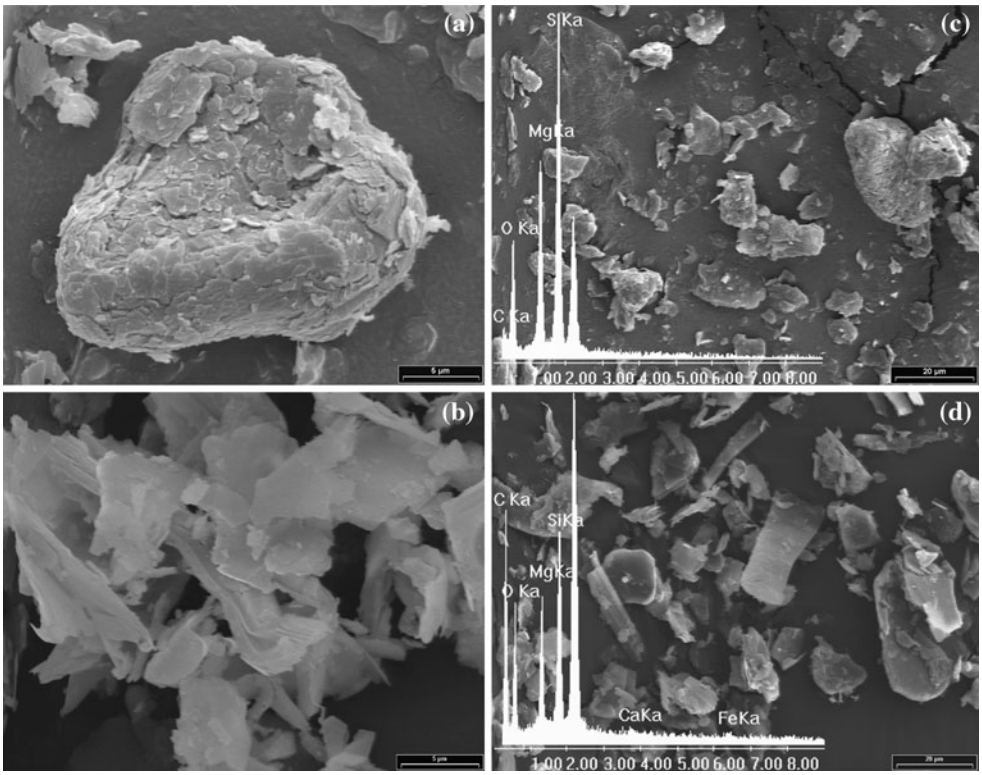

Fig. 4 SEM micrographs of initial talcs: **a** A10 and **b** SJ10 at 4000×; **c** A10 and **d** SJ10 at 1000× with EDX spectrum

hydrogen bond interactions, was revealed as a broad band at 3430 cm^{-1} [12]. Also, as the acid pH decreased a band at 3735 cm^{-1} appeared, which could be associated to the formation of isolated –SiOH groups. This is consistent with the breakage of siloxane bonds in face surfaces observed by Fraile et al. [16]. Moreover, an indication of amorphous silica formation was observed in A10-C spectrum by the presence of a band at about 781 cm^{-1}. All the acid treatments dissolved dolomite, but only HCl eliminated chlorite. HCl caused greater modifications in SJ10, dissolving all the impurities and producing the opening of tetrahedral –Si–O–Si– bonds. This was observed from the FTIR spectra of SJ10-A, SJ10-F, and SJ10-CA (Fig. 6b). Dolomite (2532, 1440, and 884 cm^{-1}) and magnesite (1440, 884, and 747 cm^{-1}) were still present after treatment in SJ10-A and SJ10-F. Likewise, the formic acid was more effective in removing associated minerals than the acetic acid; this is apparent from the lower peak heights of dolomite and magnesite bands than for SJ10-A. During the organic acid attack at least two competitive reactions took place: dissolution of associated minerals and esterification of talc –OH groups. Moreover, organic bands appeared even if the acetic acid attack was carried out on HCl treated talc, where associated minerals certainly were not present (SJ10-CA in Fig. 6b). Such grafting reaction could take place, either onto talc –OH or silanols resulting from the HCl treatment.

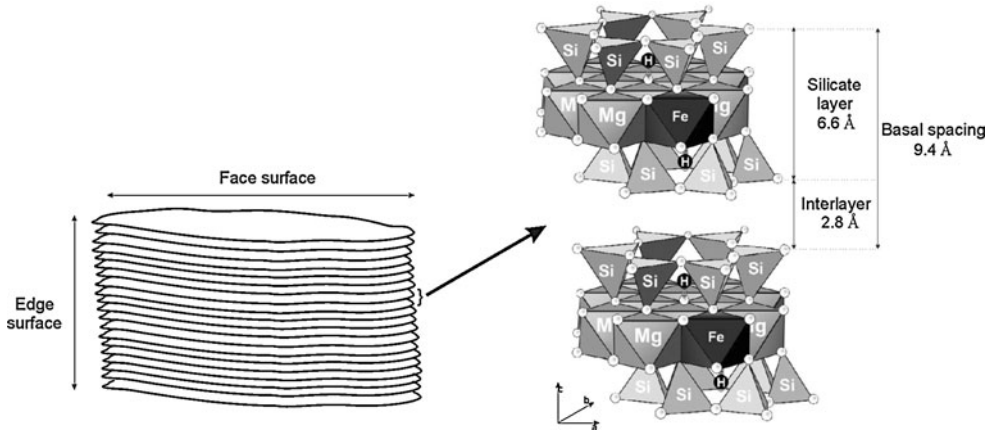

Fig. 5 Stacking structure of talc particle

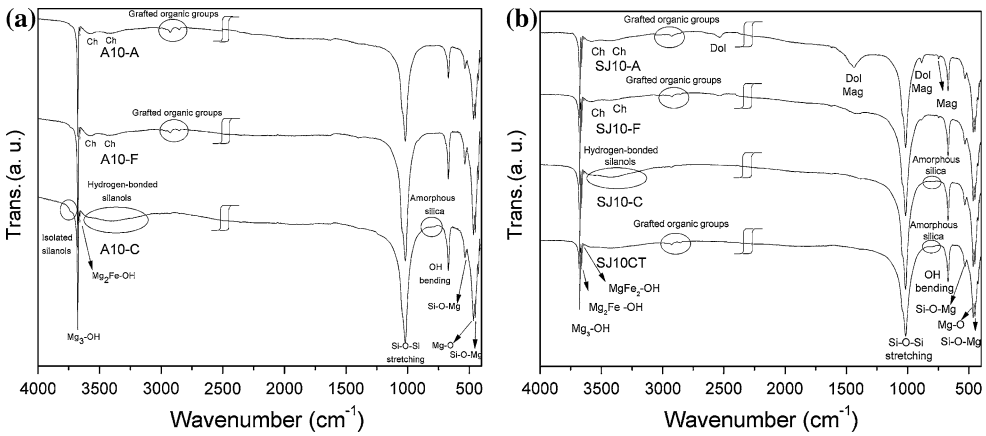

Fig. 6 FTIR spectrum of **a** A10-A, A10-F, A10-C and **b** SJ10-A, SJ10-F, SJ10-C, SJ10-CA. *Ch* chlorite, *Dol* dolomite, *Mag* magnesite

XRD was used to analyze the acid treatment effects on talc purification degree and crystallinity. The spectra of treated A10 (Fig. 7a) confirm the FTIR results; dolomite was eliminated in all samples but chlorite only in A10-C. Also, the more severe HCl treatment resulted in the intensity reduction of reflections, but did not affect their positions or their relative intensities. Since talc reflections were still present after the different acid treatments, it was possible to assume that the structure has been only partially destroyed. The balance between acid attack and structural preservation may hold the key to optimize the acid treatment conditions. The effects of acid treatments on the mineral structure of A10 samples were assessed by their *C* index variations. Table 2 presents the *C* value related to (002) basal reflections for all treatments. A decrease in C_{002} index was observed as the acid strength increases, this reduction was greater for A10-C sample. Notably, for HCl treatment the C_{002} index went down to 29%, most probably due to bonds rupture corresponding to Si-tetrahedral groups [16].

XRD from treated SJ10 (Fig. 7b) revealed that associated minerals (calcite, dolomite, chlorite, and magnesite) were completely eliminated both in SJ10-C and SJ10-CA samples, confirming the FTIR results. Likewise, the C_{002} index (Table 2) showed the greatest reduction when SJ10 was treated with HCl, again due to siloxane bonds rupture and silanol groups formation.

Surface affinity of treated talcs was evaluated by a hydrophobicity/hydrophilicity test in order to characterize the surface modifications at macroscopical level. Photographs of all talc samples inside beakers containing water and hexane are presented in Fig. 8. Densities of talc, water, and hexane are 2.78, 1, and 0.675 g/cm^3, respectively. So, talc should settle out in terms of its relatively greater density. However, two types of surfaces appear in talc particles as a result of the milling process and interlaminar slippage. Face surfaces present hydrophobic character by the presence of –Si–O–Si– groups. On the other side, edge surfaces contain hydrophilic groups as –SiOH and –MgOH. Due to this fact, initial talcs (A10 and SJ10) remained suspended at the interface, showing an amphiphilic behavior that depends on their face to edge surface ratio [7, 17].

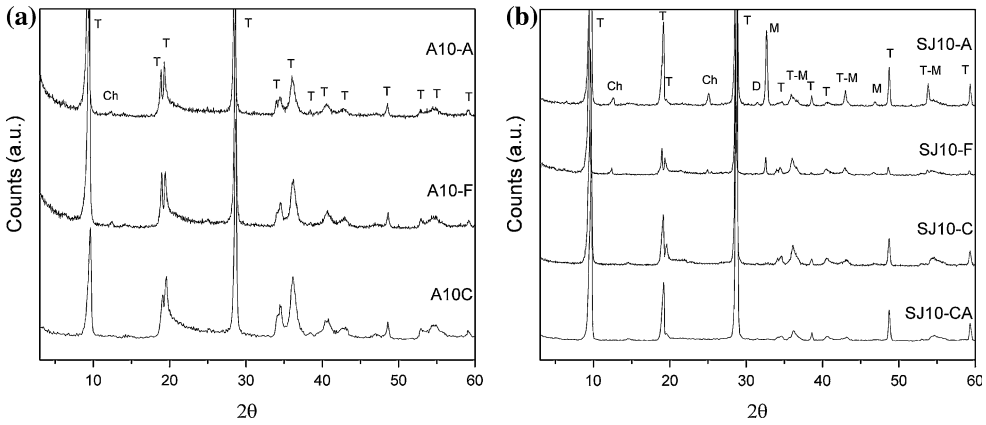

Fig. 7 X-ray spectra of treated talcs: **a** A10-A (Max. intensity: 2,252 counts), A10-F (Max. intensity: 2,485 counts), A10-C (Max. intensity: 1659 counts) and **b** SJ10-A (Max. intensity: 10,369 counts), SJ10-F (Max. intensity: 4,180 counts), SJ10-C (Max. intensity: 6,303 counts), and SJ10-CA (Max. intensity: 7,461 counts). *T* talc, *D* dolomite, *Ch* chlorite, *M* magnesite

Table 2 Crystallinity index C_{002} values of initial and treated A10 and SJ10

Talc	C_{002} (%)	Talc	C_{002} (%)
A10	100	SJ10	100
A10-A	99.10	SJ10-A	77.12
A10-F	92.75	SJ10-F	57.59
A10-C	29.05	SJ10-C	40.00
		SJ10-CA	40.18

A10-C and SJ10-C samples settled out completely, indicating that hydrophilicity was developed on their surfaces by the acid treatment. This was a clear confirmation that HCl broke siloxane bonds at the face surfaces, increasing the –OH groups content (responsible for greater water affinity).

On the other hand, for SJ10 samples treated with organic acids, a change from hydrophilic to hydrophobic character was observed only if the talc was previously purified with HCl. In this case, organic groups ($–OCOCH_3$ and –OCOH) were grafted on talc surface, giving it the hydrophobic character.

Effects on particle size

Particle splitting off and delamination of A10 and SJ10 samples were evidenced through SEM micrographs for the

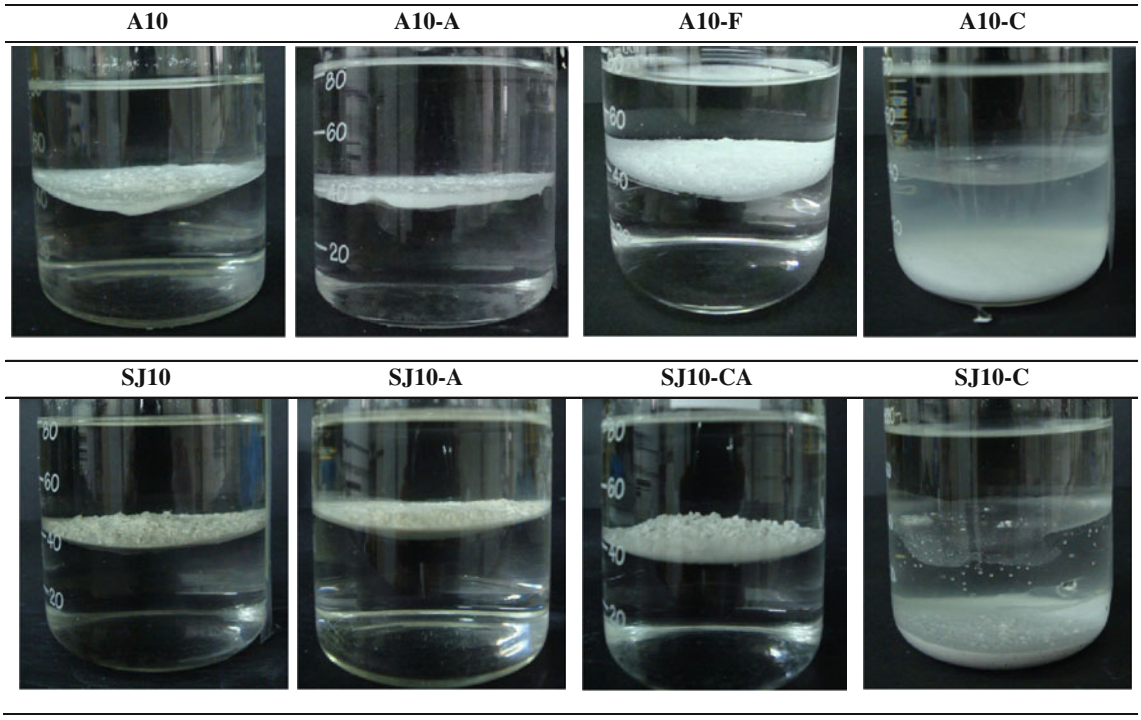

Fig. 8 Hydrophobicity/hydrophilicity tests of initial and treated talcs

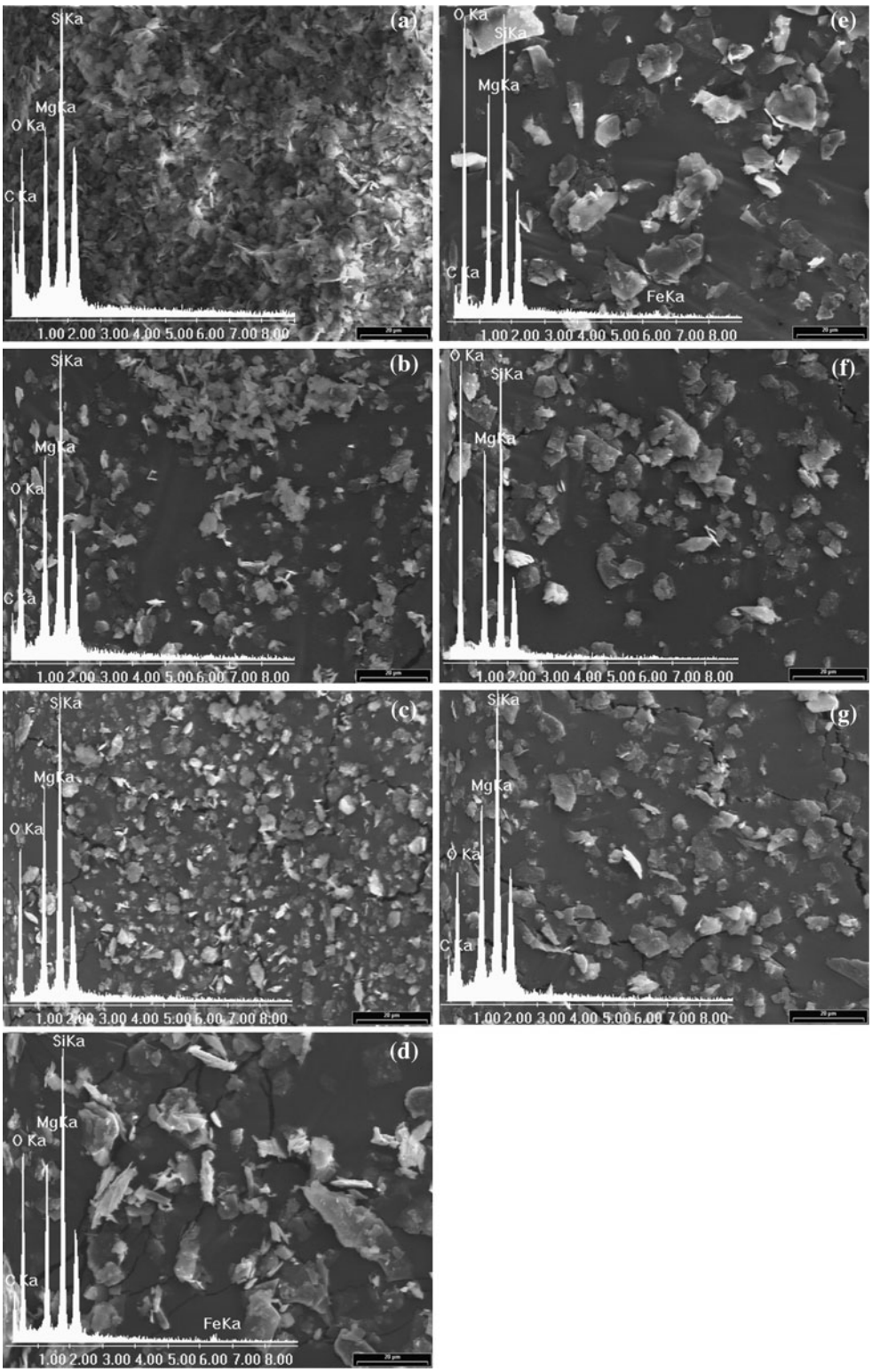

Fig. 9 SEM micrographs (1000×) of treated talcs: **a** A10-A, **b** A10-F, **c** A10-C, **d** SJ10-A, **e** SJ10-F, **f** SJ10-C, and **g** SJ10-CA with EDX spectrum

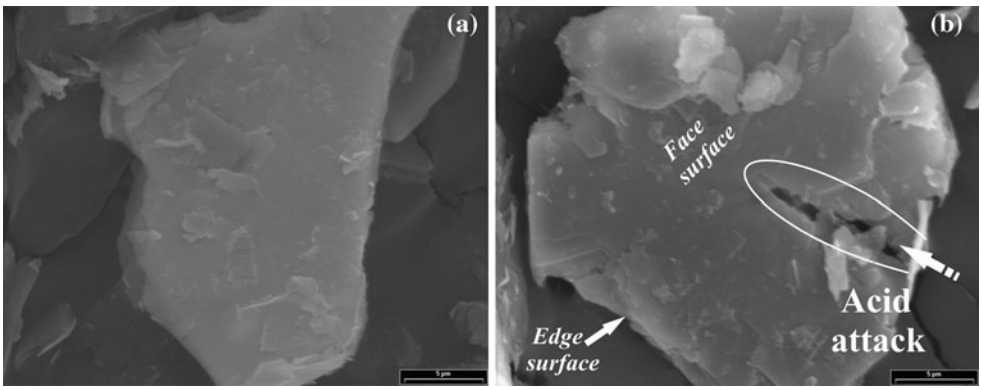

Fig. 10 SEM micrographs (4000×) of a talc particle: **a** SJ10 and **b** SJ10-C

Table 3 Mean particle length (L), thickness (e) and their percent reductions

Talc	L*(μm) ± σ	L reduction (%)	e (μm) ± σ	e reduction (%)
A10	4.53 ± 1.65	–	0.139 ± 0.016	–
A10-A	2.86 ± 1.20	36.86	0.079 ± 0.156	43.16
A10-F	2.51 ± 0.85	44.59	0.076 ± 0.036	45.32
A10-C	1.79 ± 0.43	60.49	0.069 ± 0.018	50.36
SJ10	5.85 ± 2.34	–	0.266 ± 0.173	–
SJ10-A	4.66 ± 1.56	20.51	0.154 ± 0.223	42.11
SJ10-F	4.15 ± 1.27	29.06	0.116 ± 0.052	56.39
SJ10-C	3.52 ± 0.96	39.82	0.077 ± 0.029	71.05
SJ10-CA	3.19 ± 0.86	45.47	0.073 ± 0.018	72.56

* L is the largest particle dimension

different acid treatments (Fig. 9). A *C* peak appeared in the A10-A and A10-F EDX spectra (Fig. 9a and b). This peak should correspond to the grafted organic groups since dolomite was not detected by FTIR and XRD techniques. Also, the carbon peak intensity increases notably with respect to the initial talc as can be seen by matching Fig. 9a and b with Fig. 4c. The A10-C spectrum (Fig. 9c) appeared free of Fe, Ca, and C, as it was expected from the complete solubilization of dolomite and chlorite. On the other side, the presence of Fe peak in SJ10-A and SJ10-F spectra indicated that organic acids were not able to completely eliminate chlorite (Fig. 9d and e). The *C* peak could come from either dolomite or chlorite not eliminated by CH_3COOH and HCOOH; or from the carbon grafted during the neutralization reaction. In turn, HCl acid certainly removed all the impurities since the EDX spectrum contained only the talc elements (Fig. 9f). SJ10-CA spectrum presents a *C* peak (Fig. 9g), even if it was previously treated with HCl and all the *C* content impurities eliminated. This was an unequivocal sign that carbon came from grafted organic groups.

The mechanism of acid attack can be visualized by comparing SEM micrographs of talc surfaces before and after treatment. Figure 10 illustrates the effect of acid on SJ10 talc particle surface. Acid attack started at edge surfaces by removal of Mg^{2+}, then propagated through the particle and finally was extended to other particles, producing a generalized decrease of particle size. This scheme is in agreement with the one postulated by other authors [18, 19]. The observed removal of Mg^{2+} was also consistent with the dissolution of octahedral cations (Al^{3+}) in phyllosilicates postulated by Shaw et al. [20]; particularly as they used the same pH range as in this study, and Mg^{2+} is by far more soluble in acids than Al^{3+} [21–23].

The effect of treatments on particle size (length and thickness) from A10 and SJ10 is presented in Table 3. The reduction both in particle length and thickness depended of the acid strength. Particles are more homogeneous in size as pH decreases. Comparing the measured values of A10 and SJ10 for the same acid treatments, it could be observed that the length reduction in SJ10 was lower than in A10. However, the thickness decrease was more important in SJ10. This was the result of different arrangements of associated minerals within the talc samples, as it was observed from the thin cut optical micrographs of Fig. 1. The disposition of carbonates in form of veins, with large exposed area, favored its own dissolution and helped the exposition of chlorite to acid, allowing the disaggregation and opening of talc particles. In A10, the access to talc structure by the acid was difficult since it was massive type talc, without carbonates and chlorite intergrowth.

Conclusions

Acid treatments were proposed to improve talc purity and technical properties. In particular, and related to the possible incorporation as filler in polypropylene-based composites, a considerable talc delamination and surface modification were achieved. Talcs of different origins and

composition were studied in order to assess and compare the effects of different acid treatments on their purification, delamination, particle size reduction, and surface modification.

The purity degree achieved on Argentinean talc was mainly due to the observed intergrowth of carbonates and chlorite in its structure. It presented a higher content of associated minerals with a particular carbonates spatial disposition, which helped the exposition to acid of chlorite, and allowed the disaggregation and opening of talc particles. Acid treatment allowed for the edges of particles to come apart from each other and also facilitated the dissolution of Mg^{2+} from octahedral sheets. Argentinean talc exhibited greater delamination and thus lower particle thickness than Australian one. This was a consequence of the different arrangement of associated minerals: in the first talc they were intergrowth, while the last one presented a massive structure where impurities were disposed in localized sites, hindering the acid access.

Acetate ($–OCOCH_3$) and formate (–OCOH) groups were grafted on talc surface by the proposed organic acid treatments. The occurrence of this reaction was verified by independent characterization techniques both direct (FTIR, EDX) and indirect (XRD, SEM, hydrophobicity/hydrophilicity test). Talcs treated with hydrochloric acid behaved as neatly hydrophilic, while talcs resulting from organic acid treatments were hydrophobic.

Hydrochloric acid treatment allowed for a length and thickness reduction of talc particles, the complete elimination of associated minerals and the change to hydrophilic character by breakage of siloxane bonds. The so-treated Argentinean talc achieved a purity level enough to be used in plastic and paper industry, paints, and cosmetic among other upgraded talc applications.

Acknowledgements The authors acknowledge financial support from the following institutions from Argentina: Consejo Nacional de Investigaciones Científicas y Técnicas (CONICET), Agencia de Promoción Científica y Tecnológica (ANPCyT), and Universidad Nacional del Sur (UNS).

References

1. Averous L, Quantin JC, Lafon D, Crespy A (1994) Acta Stereol 14:69
2. Averous L, Quantin JC, Lafon D, Crespy A (1995) Int J Polym Anal Charact 1:339
3. Rybnikar F (1989) J Appl Polym Sci 38:1479
4. Pukánszky B, Belina K, Rockenbauer A, Maurer FHJ (1994) Composites 25:205
5. Alonso M, Velasco JI, de Saja JA (1997) Eur Polym J 33:255
6. Vesely D, Ronca G (2001) J Microsc 201:137
7. Steen WP (1999) In: Karian HG (ed) Handbook of polypropylene and polypropylene composites, 2nd edn. Basel, New York
8. Shanks RA, Tiganis BE, Long Y (1996) Nucleation of crystallization in filled polymer blends. In: ANTEC '96 conference proceedings, Indianapolis, pp 1744–1450
9. Alonso M, Gonzalez A, de Saja JA (1995) Plast Rubber Compos Process Appl 24:131
10. Shao W, Wang Q, Li K (2005) Polym Eng Sci 45:451
11. Karrad S, Lopez Cuesta JM, Crespy A (1998) J Mater Sci 33:453. doi:10.1023/A:1004392318226
12. Taranco J, Laguna O, Artiaga RP, Collar EP, Martínez JMG (1993) Rev Plast Mod 66:415
13. Ohlberg SM, Strickler DW (1962) J Am Ceram Soc 45:170
14. Feng D, Aldrich C (2004) Ind Eng Chem Res 43:4422
15. Comard MP, Calvet R, Balard H, Dodds JA (2004) Colloids Surf A 238:37
16. Fraile JM, García JI, Mayoral JA, Vispe E (2004) Appl Catal A 276:113
17. Xanthos M (2005) Functional fillers for plastics. Wiley-VCH Verlag GmbH & Co, KGaA, Weinheim
18. Lin FC, Cemency CV (1981) Am Min 66:801
19. Saldi G, Kohler S, Marty N, Oelkers E (2007) Geochim Cosmochim Acta 71:3446
20. Shaw SA, Peak D, Hendry MJ (2009) Geochim Cosmochim Acta 73:4151
21. Corma A, Mifsud A, Sanz E (1987) Clay Miner 22:225
22. Luce RW, Bartlett WB, Parks GA (1972) Geochim Cosmochim Acta 36:35
23. Rice NM, Strong LW (1974) Can Metall 13:485